A Unified Statistical Approach for Determining Significant Signals in Images of Cerebral Activation

K.J. Worsley, S. Marrett, P. Neelin, A.C. Vandal, K.J. Friston and A.C. Evans

Department of Mathematics and Statistics, McGill University, 805 Sherbrooke St. West, Montreal, Québec, Canada H3A 2K6 (K.J.W., A.C.V), McConnell Brain Imaging Centre, Montreal Neurological Institute, 3801 University St., Montreal, Québec, Canada H3A 2B4 (S.M., P.N., A.C.E.) and The Welcome Department of Cognitive Neurology, Queen Square, London, UK WC1N 3BG (K.J.F.)

Abstract: We present a unified statistical theory for assessing the significance of apparent signal observed in noisy difference images. The results are usable in a wide range of applications, including astrophysics, but are discussed with particular reference to images which represent changes in cerebral blood flow elicited by a specific cognitive or sensorimotor task. Our main result is an estimate of the p-value for local maxima of Gaussian, t, χ^2 and F fields over search regions of any shape or size in any number of dimensions. This unifies the p-values for large search areas in 2-D (Friston *et al.* 1991), large search regions in 3-D (Worsley *et al.* 1992), and the usual uncorrected p-value at a single pixel or voxel.

Key words: PET, fMRI, Euler characteristic, random fields.

Addresses of corresponding author:
e-mail: keith@zaphod.math.mcgill.ca
ph: 1-514-398-3842
fax: 1-514-398-3899.

1 Introduction

Many studies of brain function with positron emission tomography (PET) involve the interpretation of a subtracted PET image, usually the difference between two images of cerebral blood flow (CBF) under baseline and activation conditions. In general a series of up to 12 seperate conditions are measured in each subject. In many cognitive studies, the activation is so slight (4-8%) that the experiment must be repeated on several subjects. The images are then mapped into a standardised coordinate space to account for differences in brain size and orientation, and the subtracted images averaged to improve the signal to noise ratio (Fox *et al.* 1985; Friston *et al.* 1990, 1991; Evans *et al.* 1992; Worsley *et al.* 1992). The averaged ΔCBF image is then normalised by dividing by an estimate of the standard deviation and the resulting statistical field or parametric map is searched for local maxima. The standard deviation can be estimated either by pooling error sum of squares over subjects and conditions (Friston *et al.* 1990), or by pooling over subjects and voxels (Worsley *et al.* 1992). In Section 2 we suggest a unified estimator which has the advantages of both.

In either case the main problem is to determine the significance of extrema in the statistical field. For a Gaussian statistical field, Friston *et al.* (1991) give results for a 2-D search region, Worsley *et al.* (1992) give results for a 3-D search region, and Worsley *et al.* (1993) extend this to a 3-D t statistical field. These results are accurate only for search regions larger than 100cc; the purpose of the present paper is to give a better approximation for search regions of any shape or size. This makes it possible to restrict the search to small anatomical regions such as the cingulate gyrus or caudate nucleus, or two dimensional regions such as a slice or the cortical surface, or even single voxels. Previous results for 2-D searches (Friston et al. 1991) are included as a special case. The results are also generalisable to 4-D searches in time as well as space, which may be useful for functional MRI (Kwong *et al.* 1992; Ogawa *et al.* 1992; Friston *et al.* 1994, Ouyang *et al.* 1994). The unified p-value is given in Section 3 and validated in Section 4. We present some applications in Section 5 and a discussion in Section 6. Extensions to regression models and χ^2 and F fields are elaborated in the Appendix.

2 The statistical field

2.1 Modelling the data

In a typical CBF activation study, PET image data are collected from $n > 1$ subjects under a set of $m > 1$ conditions or tasks. Let $C^*_{ij}(x, y, z)$ be the CBF of subject i under condition j, $i = 1, \ldots, n$, $j = 1, \ldots, m$ at voxels with coordinates (x, y, z) and let G^*_{ij} be the global mean of all intracranial voxels. The asterisk is used to emphasise that these parameters are in absolute units.[1] The 'independent' ANCOVA model of Friston *et al.* (1990) is

$$C^*_{ij}(x, y, z) = r(x, y, z)G^*_{ij} + \delta^*_j(x, y, z) + \epsilon^*_{ij}(x, y, z), \tag{2.1}$$

where $r(x, y, z)$ is a regression coefficient common to all subjects and conditions, $\delta^*_j(x, y, z)$ is a condition specific change in blood flow and $\epsilon^*_{ij}(x, y, z)$ is an error term normally distributed

[1] Friston *et al.* (1990) use i for voxel coordinates, j for subjects and k for conditions

with a mean of zero. In practice the ANCOVA model is usually extended to include a block or subject specific term $a_i^*(x,y,z)$ which represents an underlying blood flow for subject i (Friston *et al.* 1991, 1994b):

$$C_{ij}^*(x,y,z) = r(x,y,z)G_{ij}^* + a_i^*(x,y,z) + \delta_j^*(x,y,z) + \epsilon_{ij}^*(x,y,z). \tag{2.2}$$

The degrees of freedom for the ANCOVA model (2.2) is $\nu = (n-1)(m-1)-1$.

Let $Y_{ij}(x,y,z) = C_{ij}^*(x,y,z)/G_{ij}^*$ be the normalised blood flow. Then the model (2.2) can be written as

$$Y_{ij}(x,y,z) = r(x,y,z) + \frac{a_i^*(x,y,z) + \delta_j^*(x,y,z) + \epsilon_{ij}^*(x,y,z)}{G_{ij}^*}. \tag{2.3}$$

where $r(x,y,z)$ can be interpreted as an underlying normalised blood flow common to all subjects and conditions. The ANOVA model (Fox *et al.* 1988; Worsley *et al.* 1992) is

$$Y_{ij}(x,y,z) = r(x,y,z) + a_i(x,y,z) + \delta_j(x,y,z) + \epsilon_{ij}(x,y,z) \tag{2.4}$$

where $a_i(x,y,z)$ is an underlying normalised blood flow for subject i, $\delta_j(x,y,z)$ is a condition specific change in normalised blood flow and $\epsilon_{ij}(x,y,z)$ is an error term normally distributed with a mean of zero. The degrees of freedom for the ANOVA model is $\nu = (n-1)(m-1)$. If the global means G_{ij}^* are equal for all subjects and conditions then the models (2.2), (2.3) and (2.4) are identical, up to multiplication by a constant; note that the first term in (2.2) is then absorbed into the constant term and the degrees of freedom increases to $\nu = (n-1)(m-1)$.

To make the presentation simpler, we shall work with the ANOVA model; a similar development can be made for the ANCOVA model without any extra theoretical difficulty. Suppose we are interested in testing for a particular contrast of the responses,

$$\delta(x,y,z) = \sum_j c_j \delta_j(x,y,z), \tag{2.5}$$

where the coefficients $\{c_1,\ldots,c_m\}$ are chosen so that $\sum_j c_j = 0$. For example, to test for a difference between the first and second conditions we could use $\{c_1,\ldots,c_m\} = \{-1,1,0,\ldots,0\}$; to test for a difference between the average of the first two conditions and the average of the next two conditions we could use $\{c_1,\ldots,c_m\} = \{-1,-1,1,1,0,\ldots,0\}$; to test for a time trend we could use $c_j = j - (m+1)/2$; to test for correlation with stimulus intensity we could let c_j be the stimulus intensity normalised so that $\sum c_j = 0$. The effect of this contrast on subject i, normalised to keep the standard deviation equal to that of the observations, is

$$\Delta_i(x,y,z) = \sum_{j=1}^m c_j Y_{ij}(x,y,z) \Big/ \left[\sum_{j=1}^m c_j^2\right]^{1/2}. \tag{2.6}$$

For example, a simple two condition subtraction is

$$\Delta_i(x,y,z) = [Y_{i2}(x,y,z) - Y_{i1}(x,y,z)]/\sqrt{2}. \tag{2.7}$$

The overall effect on all subjects, again normalised to keep the standard deviation equal to that of the observations, is

$$\Delta(x,y,z) = \sum_{i=1}^n \Delta_i(x,y,z)/n^{1/2}, \tag{2.8}$$

which for a two condition subtraction is

$$\Delta(x,y,z) = \sum_{i=1}^{n} [Y_{i2}(x,y,z) - Y_{i1}(x,y,z)]/\sqrt{2n}. \tag{2.9}$$

Thus $\Delta(x,y,z)$ can be regarded as a generalised ΔCBF image. Note that it is straightforward to generalise still further to arbitrary c_{ij} (see Friston *et al.* 1994b) but this will not be studied further in this paper. Extensions to regression models for subject specific regressors is possible within the framework of this paper, and the details are developed in the Appendix.

The remaining question is how to find a suitable estimator for the variance of $\Delta(x,y,z)$. In the Appendix we show that a high accuracy estimator is essential for good sensitivity. The only way of obtaining such an estimator is to pool information about the variance from different sources and, to do this, some assumption must be made about the behaviour of the true population variance. We shall start by assuming that the variance and covariance of the error term, for a given subject at a given voxel, depend both on the voxel position and on the condition, but not on the subject:

$$\mathrm{Cov}[\epsilon_{ij}(x,y,z), \epsilon_{ik}(x,y,z)] = \sigma^2_{jk}(x,y,z), \tag{2.10}$$

where j and k are two conditions, $j,k = 1,\ldots,m$. This model allows for the possiblity that the variance may be different in different brain regions and under different conditions, and that the conditions j and k may be correlated due perhaps to repeated testing over time, but it does assume that the variance-covariance structure is identical for every subject. It can be shown that a departure from this last assumption slightly reduces the sensitivity of the statistical field but does not appreciably affect its specificity. Then an unbiased estimator of the variance of $\Delta(x,y,z)$ is

$$\sum_{i=1}^{n} [\Delta_i(x,y,z) - \Delta(x,y,z)]^2/(n-1), \tag{2.11}$$

which depends on the particular contrast chosen. This estimator is unaffected by either differences in the voxel variance, or differences in the condition variance, but unfortunately it has rather low degrees of freedom $(n-1)$, since the number of subjects in a typical experiment is usually small. Two methods have been proposed for overcoming this.

2.2 Pooling over conditions

Friston *et al.* (1991) proposed pooling over conditions to increase the degrees of freedom. This is valid provided the condition variances are equal and the condition covariances are zero, that is provided

$$\sigma^2_{jj}(x,y,z) = \sigma^2(x,y,z) \quad \text{and} \quad \sigma^2_{jk}(x,y,z) = 0, \tag{2.12}$$

$j \neq k$. A better variance estimator can then be obtained by averaging (2.11) over all $(m-1)$ orthogonal contrasts $\{c_1,\ldots,c_m\}$. This is equivalent to the usual ANOVA mean error sum of squares

$$s^2(x,y,z) = \sum_{i=1}^{n}\sum_{j=1}^{m} [Y_{ij}(x,y,z) - \bar{Y}_{i\bullet}(x,y,z) - \bar{Y}_{\bullet j}(x,y,z) + \bar{Y}_{\bullet\bullet}(x,y,z)]^2/\nu \tag{2.13}$$

where, using the standard notation,

$$\begin{aligned}
\bar{Y}_{i\bullet}(x,y,z) &= \sum_{j=1}^{m} Y_{ij}(x,y,z)/m, \\
\bar{Y}_{\bullet j}(x,y,z) &= \sum_{i=1}^{n} Y_{ij}(x,y,z)/n, \\
\bar{Y}_{\bullet\bullet}(x,y,z) &= \sum_{i=1}^{n}\sum_{j=1}^{m} Y_{ij}(x,y,z)/(nm), \\
\nu &= (n-1)(m-1). \qquad (2.14)
\end{aligned}$$

Dividing $\Delta(x,y,z)$ by $s(x,y,z)$ produces the statistical field

$$T(x,y,z) = \Delta(x,y,z)/s(x,y,z), \qquad (2.15)$$

which has a t-distribution with ν degrees of freedom when no activation is present. We shall see later in Section 3.4 that ν must be greater than three to avoid singularities in the statistical field.

The advantage of this approach is that it allows for unequal voxel standard deviations; the disadvantages are that it does not allow for unequal condition standard deviations, and the low degrees of freedom can reduce the sensitivity.

2.3 Pooling over voxels

Worsley *et al.* (1992) have assumed that the variance is equal across all voxels, that is

$$\sigma^2_{jk}(x,y,z) = v_{jk}\sigma^2 \qquad (2.16)$$

where v_{jk} is a scaling factor to allow for unequal condition variances and covariances, and σ^2 is a common image variance. Then we can pool over subjects and the N voxels in the search region to obtain

$$S_c^2 = \sum_{i=1}^{n}\sum_{x,y,z} [\Delta_i(x,y,z) - \Delta(x,y,z)]^2/[(n-1)N], \qquad (2.17)$$

where the subscript c without (x,y,z) emphasises the fact that this estimator depends on the contrast but not on the voxel. The statistical field based on this pooled standard deviation is

$$Z(x,y,z) = \Delta(x,y,z)/S_c. \qquad (2.18)$$

If the search region is large with respect to the effective FWHM then the degrees of freedom of S_c is very large and so the distribution of $Z(x,y,z)$ can be well approximated by a normal distribution with unit variance (Worsley *et al.* 1992).

The advantages of this approach are that the high effective degrees of freedom give improved sensitivity, and it allows for unequal condition standard deviations. The disadvantage is that it does not allow for unequal voxel standard deviations.

2.4 A combined model

An estimator which combines the advantages of both approaches is based on the assumption that the variance is a product of the condition factor v_{jk} and the voxel variance $\sigma^2(x,y,z)$:

$$\sigma^2_{jk}(x,y,z) = v_{jk}\sigma^2(x,y,z). \tag{2.19}$$

It can be shown that an approximately unbiased estimator of the variance of $\Delta(x,y,z)$ is

$$s^2_c(x,y,z) = [S^2_c/S^2]s^2(x,y,z) \tag{2.20}$$

where

$$S^2 = \sum_{x,y,z} s^2(x,y,z)/N. \tag{2.21}$$

is the variance pooled over all conditions and voxels. (Note that S^2 is also the average of S^2_c over all orthognal condition contrasts.) This estimator in effect scales the voxel variance by the factor S^2_c/S^2 so that its average matches the pooled condition variance. If the search region is large with respect to the effective FWHM then this scaling factor is approximately constant and so the degrees of freedom of $s^2_c(x,y,z)$ is approximately ν. The distribution of the statistical field

$$T_c(x,y,z) = \Delta(x,y,z)/s_c(x,y,z) \tag{2.22}$$

can be well approximated by a t distribution with $\nu = (n-1)(m-1)$ degrees of freedom. This statistical field should avoid some of the problems of either of the previous two, namely a dependence on equality over either conditions or voxels, but once again it does depend on an assumed multiplicative model for the variance which may not be correct. This statistical field is closer in spirit to $T(x,y,z)$, but the problem of low sensitivity caused by low degrees of freedom still remains (see Appendix).

If the ANCOVA model (2.2) is used then similar methods can be used to obtain statistical fields analogous to (2.15), (2.18) and (2.22). The main difference is that $\nu = (n-1)(m-1)-1$ should be used throughout.

3 A unified formula for the p-value of statistical field extrema

3.1 The formula

Throughout this section we will be concerned with the p-value of the maximum M of the statistical field inside a search region V. There is, as yet, no known exact result for the p-value of M (Adler, 1981, Chapter 6). However exact results have recently been found for the expected *Euler characteristic* (EC) of the *excursion set* of an isotropic statistical field. The excursion set is simply the set of voxels where the statistical field exceeds a fixed threshold t and the EC counts the number of connected components of the excursion set, minus the number of 'holes' plus the number of 'hollows' (see Worsley *et al.* 1992). For high thresholds the holes and hollows disappear and the EC counts the number of local maxima of the statistical field. For even higher thresholds, near the global maximum M, the EC

counts one if $M \geq t$ and zero otherwise, so that the expected EC approximates the p-value of M. The expected EC is therefore our proposed unified formula for the p-value:

$$\mathrm{P}(M \geq t) \approx \sum_{d=0}^{3} R_d(V)\rho_d(t). \tag{3.1}$$

We shall give exact definitions of the coefficients in the formula in the following sections, but a rough description now follows. The mathematical derivations behind (3.1) are presented in Worsley (1995a), and this paper attempts only to give an intuitive review of the results. The *resel count* $R_d(V)$ is a unitless quantity which depends only on certain d-dimensional features of the search region V in *resel space* (see Sections 3.2 and 3.3), and the *EC density* $\rho_d(t)$ depends only on the threshold t and the type of statistical field (see Section 3.4). The $d = 3$ term, usually the largest, is identical to the 3-D p-value of Worsley *et al.* (1992); the $d = 2$ term is (after correction by $\pi/4$) half the 2-D p-value of Friston *et al.* (1991) applied to the surface area of V in resel space; the $d = 1$ term is a 1-D analogue, and the $d = 0$ term is, when V is convex, the p-value of the statistical field at a single voxel.

The above p-value is *unified* because we shall impose essentially no restrictions on V (see Discussion); it can be a 3-D volume of arbitrary shape, a 2-D slice, a 2-D surface (such as the cortical surface), a 1-D line or a 0-D point; it can be connected or disconnected. Extensions to 4-D, for example space and time, are possible; see Section 3.6. However the above approximation (3.1) is best when the search region is convex, and it appears to be accurate for high thresholds t whenever the p-value is less than 0.2. For lower thresholds, (3.1) approximates the expected number of false positive peaks in the image above t.

For the validity of the unified p-value, we shall require that $\epsilon_{jk}(x, y, z)/\sigma_{jk}(x, y, z)$ be a stationary Gaussian random field with zero mean and unit variance, generated by smoothing white noise with the point response function of the PET camera. Stationarity then implies that the point spread function should be the same at all positions in the aperture of the PET camera. Finally, we shall assume that the point spread function is itself Gaussian with FWHMs w_x, w_y and w_z in the x, y and z directions (see Friston *et al.* 1991; Worsley *et al.* 1992). This last assumption need only hold near the peak of the point spread function, since our results depend only on the curvature of the point spread function at its peak and not on its behaviour in the tails.

3.2 Resel counts for continuous data

In this section we shall assume that the search region V is continuous, such as a sphere or cube. We shall first transform V into *resel space* by dividing the coordinates of the voxels (x, y, z) by the FWHMs in the corresponding directions (w_x, w_y, w_z), so that the statistical field becomes *isotropic*. In practice this can easily be achieved by re-defining the voxel sizes $d_x \times d_y \times d_z$ to be $r_x \times r_y \times r_z$ where $r_x = d_x/w_x$, $r_y = d_y/w_y$ and $r_z = d_z/w_z$. The use of resel space instead of voxel space emphasises the dependence of statistical properties on the fixed physical dimensions of the point spread function, as opposed to the arbitrarily specified voxel dimensions. Note that this makes all measurements in resel space *unitless*. We then define:

- The *resel volume* $R_3(V)$ is the volume of V in resel space. This can be calculated quite simply by dividing the volume of V by the product $w_x w_y w_z$; note that this equals the number of RESELS in V as defined by Worsley *et al.* (1992).

- The *resel surface area* $R_2(V)$ is the half surface area of V in resel space. If V is a 2-D surface, either flat or curved, such as a slice, then the two 'sides' of V combine and $R_2(V)$ is just the area of V in resel space.

- The *resel diameter* $R_1(V)$ is, if V is convex, twice the average caliper diameter of V in resel space, that is, the average over all rotations of the distance between two parallel planes tangent to V in resel space, or, twice the average width of all bounding boxes of V in resel space. If V is a 2-D surface then $R_1(V)$ is half the perimeter length of V in resel space. If V is a 1-D line, straight or curved, then $R_1(V)$ is just the length of V in resel space.

- $R_0(V)$ is the EC of V; this is the same whether it is measured in resel space or not.

Some examples are given in Table 1; values for some other common geometric solids can be found in Santaló (1976), page 229.

3.3 Resel counts for voxel data

Throughout the previous section the search region was regarded as a region with a smooth boundary defined at every point in 3-D. In practice only voxel data is available, and this will be regarded as a continuous image sampled on a lattice of equally spaced points. Thus a voxel is treated as a *point* in 3-D with zero volume, although it is often displayed on computer screens and in publications as a *volume* centred at that point.

The following method shows how to approximate the resel counts from voxel data without actually transforming to resel space. The degree of approximation improves as the boundary of the search region approaches the boundary of the voxels, and the approximation is exact if they coincide. Suppose the voxels are labelled v_{ijk}, where i, j and k are integers labelling the voxels along the x, y and z axes respectively; see Figure 1 for a simple example.

- Let P be the number of voxels in V.

- Let E_x be the number of x-direction 'edges' in V, that is the number of pairs of adjacent voxels $\{v_{ijk}, v_{i+1,j,k}\}$ both of which are in V.

- Let E_y be the number of y-direction edges in V, that is the number of pairs of adjacent voxels $\{v_{ijk}, v_{i,j+1,k}\}$ both of which are in V.

- Let E_z be the number of z-direction edges in V, that is the number of pairs of adjacent voxels $\{v_{ijk}, v_{i,j,k+1}\}$ both of which are in V.

- Let F_{xy} be the number of 'faces' of four adjacent voxels in the x and y directions, $\{v_{ijk}, v_{i+1,j,k}, v_{i,j+1,k}, v_{i+1,j+1,k}\}$, all of which are in V.

- Let F_{xz} be the number of faces of four adjacent voxels in the x and z directions, $\{v_{ijk}, v_{i+1,j,k}, v_{i,j,k+1}, v_{i+1,j,k+1}\}$, all of which are in V.
- Let F_{yz} be the number of faces of four adjacent voxels in the y and z directions, $\{v_{ijk}, v_{i,j+1,k}, v_{i,j,k+1}, v_{i,j+1,k+1}\}$, all of which are in V.
- Let C be the number of 'cubes' of eight adjacent voxels, all of whose vertices $\{v_{ijk}, v_{i+1,j,k}, v_{i,j+1,k}, v_{i+1,j+1,k}, v_{i,j,k+1}, v_{i+1,j,k+1}, v_{i,j+1,k+1}, v_{i+1,j+1,k+1}\}$ are in V.

Then

$$\begin{aligned} R_0(V) &= P - (E_x + E_y + E_z) + (F_{yz} + F_{xz} + F_{xy}) - C, \\ R_1(V) &= (E_x - F_{xy} - F_{xz} + C)r_x + (E_y - F_{xy} - F_{yz} + C)r_y + (E_z - F_{xz} - F_{yz} + C)r_z, \\ R_2(V) &= (F_{xy} - C)r_x r_y + (F_{xz} - C)r_x r_z + (F_{yz} - C)r_y r_z, \\ R_3(V) &= C r_x r_y r_z. \end{aligned} \tag{3.2}$$

For example, an $I \times J \times K$ voxel box shaped search region gives

$$\begin{aligned} R_0(V) &= 1, \\ R_1(V) &= (I-1)r_x + (J-1)r_y + (K-1)r_z, \\ R_2(V) &= (I-1)(J-1)r_x r_y + (I-1)(K-1)r_x r_z + (J-1)(K-1)r_y r_z, \\ R_3(V) &= (I-1)(J-1)(K-1)r_x r_y r_z. \end{aligned} \tag{3.3}$$

Note again that *for the purposes of these calculations*, a single $1 \times 1 \times 1$ voxel has zero volume, surface area and diameter. A $2 \times 2 \times 2$ voxel search region is the smallest that has positive resel volume. Since the search region defined by voxels has a non-convex 'jagged' boundary then the resel counts of a voxel region tend to be larger than that of the equivalent smoothed region. However in practice these discrepancies do not appear to affect the formulas, unless the region is 'badly placed', such as a rectilinear or flat region which is not aligned with the voxel axes.

3.4 EC densities

Under the assumptions of Section 2.3 it can be shown that $Z(x, y, z)$ is a stationary Gaussian random field. Let $\phi(t)$ be the density of the standard Gaussian distribution. Then the EC densities for this statistical field are given in Table 2(a) (Adler, 1981; Worsley *et al.* 1992). Under the assumptions of Section 2.2 it can be shown that $T(x, y, z)$ is a stationary t random field, and under the assumptions of Section 2.4 it can be shown that $T_c(x, y, z)$ is a stationary t random field. The EC densities for these statistical fields are given in Table 2(b) (Worsley, 1994).

Note that singularities can occur in a t-field if $\nu < d$. The reason for this is a curious property of χ^2 fields. For $\nu < d$ the χ^2 field in the denominator can have exact zeros which produce exact positive and negative inifinities in the t-field, in which case the maximum M is infinite with positive probability. In practice these singularities fall between the voxels and would only be observed if the images were interpolated between voxel locations. Their presence would still be felt by large fluctuations in neighbouring voxel values.

Note also that it is *not* possible to transform a t field to a Gaussian field by simply transforming the field to a Gaussian distribution at each voxel. That this is so can be seen from the fact that the t-field for $\nu < d$ can have exact zeros, whereas a smooth Gaussian field cannot. For large degrees of freedom, Friston *et al.* (1991) have used this as an approximation; in the Appendix we show that this is sufficiently accurate if $\nu > 120$, although $\nu > 40$ appears reasonable.

3.5 Examples

Figure 2 plots critical t thresholds of M for a Gaussian statistical field with FWHMs $w_x = w_y = w_z = 20$mm. Two search regions were chosen; a spherical search region with radius $x$cm and a cubical search region with the same volume. Since the FWHMs are equal, transforming to resel space simply divides the size by 2cm, so the sphere has radius $r = x/2$ in resel space. The unified p-value for the sphere is, from Table 1,

$$\mathrm{P}(M \geq t) \approx \rho_0(t) + 4r\rho_1(t) + 2\pi r^2\rho_2(t) + (4/3)\pi r^3\rho_3(t). \tag{3.4}$$

The p-value was equated to 0.1, 0.05 and 0.01 to find the approximate critical thresholds t at these false positive rates. As the size decreases the critical values decrease down to the usual Gaussian critical values at a single point: 1.28, 1.64 and 2.33, respectively. The cube gives values slightly larger than the sphere, which is a lower bound for all search regions of the same volume. Below these are 2-D results for a disk of radius x and a square of the same area, which behave in a similar way. Also shown are the approximate large volume critical values of Worsley *et al.* (1992) which equal the first term of the unified p-value, plotted only for large values of x; they are slightly lower than those given by the unified p-value. Figure 3 repeats this for a t statistical field with $\nu = 40$ degrees of freedom, drawn to the same scale; the same patterns are evident, but the critical thresholds are larger.

3.6 Searches over space and time

Data from fMRI can be represented as a statistical field in four dimensions: three space dimensions and one time dimension. We may be interested in searching for peaks of activation somewhere in a region of the brain V that occurred at an unknown time in an interval of length T. Let w_t be the FWHM of the haemodynamic response function (Friston *et al.* 1994a) and let $\tau = T/w_t$ be the time interval measured in *time resels*. Then it can be shown (Worsley, 1995ab) that the unified p-value is

$$\mathrm{P}(M \geq t) \approx \sum_{d=0}^{3} R_d(V)[\tau\rho_{d+1}(t) + \rho_d(t)]. \tag{3.5}$$

All the resel counts and EC densities are the same as before; the only new requirement is the 4-D EC density which is given in Table 2.

4 Validation

To validate the critical values given by the unified p-value, 200 3-D Gaussian statistical fields were generated by smoothing independent zero mean Gaussian random variables at $64 \times 64 \times$

64 voxels with a nominal separation of 2.1mm, using a Gaussian point spread function with FWHM=20mm. Three different search region shapes were chosen: a $2a \times 2a \times 2a$ cube, a flat $2a \times 2a \times a$ 'pizza box', and a thin $2a \times a \times a$ 'shoe box'. The maximum size of the search regions was restricted to half the size of the statistical field to avoid the wrap-around effects from the Fourier smoothing. Each statistical image was then 'smoothed' with a 3-D max filter which had the same shape as the search region, that is, the search region was centred at every voxel and the maximum inside the search region provided a 'smoothed' value at that voxel. The box shaped search regions allowed us to speed up the calculations by applying a 1-D max filter along the x, y and z axes in turn.

The histogram of the max filtered image estimates the distribution of M, and the upper percentiles were used to estimate critical values of M. These are plotted in Figures 4, 5 and 6 for the three search regions. Agreement with the theoretical values, calculated according to (3.1), (3.3) and Table 2(a), seems very good, apart from some deviations for large regions. This can be explained by a 'partial volume' effect for the max filtered image; when the search region is large the max filtered voxels are highly correlated and so the effective number of independent simulated values is reduced, thus increasing the deviations. Note also that the same filtered images were used for each search region, so points on the graphs are highly correlated, which tends to exagerate any apparent trends in the deviations. Simulations are, however, independent between search regions.

5 Application

Thresholds of M for several different structures are shown in Table 3. To illustrate the methods of this paper, the resolution was taken as FWHM=20mm in each direction, and thresholds were calculated for the maximum of a Gaussian image at three different false positive rates. The smaller structures were obtained from a voxel atlas of the left hemisphere of the brain (Evans *et al.* 1991), and the whole brain region included the grey matter and all interior structures. A 4mm thick shell around the whole brain was used to represent a search in the outer cortex. A single voxel is included for comparison.

Even though the smaller structures have a small volume, the thresholds are appreciably higher than those for a single voxel. Lack of smoothness in their boundaries causes some structures to have quite large resel surface area ($R_2(V)$) and resel diameter ($R_1(V)$), and an Euler characteristic ($R_0(V)$) that is different from 1. Nevertheless, some elongated structures such as the cingulate gyrus have high surface area and diameter relative to their volume. This gives the cingulate gyrus the same thresholds as the superior parietal lobule, which has a 62% greater volume but a 38% smaller diameter. Note that if the search is confined to a thin shell the thresholds are considerably reduced from that for the whole brain, since the search region is almost two-dimensional with resel volume close to zero. Note that the resel surface area of the shell is approximately twice that of the whole brain, and the shell's Euler characteristic is 2, 1 for the outside and 1 for the 'hollow'.

6 Discussion

The unified p-value of M combines features from all dimensions d of V. For large regions the $d = 3$ term is the most important, but if the region is flat then the $d = 3$ term vanishes and the $d = 2$ term dominates; half the surface area from both sides of the region gives just the area of V and so the $d = 2$ term becomes the usual 2-D result. If the region collapses to a single voxel then the $d = 1, 2, 3$ terms are all zero and the $d = 0$ term gives just the p-value at a single point. Thus the unified formula has the correct behaviour for all dimensions from 0-D to 3-D. This behaviour stems from the fact that the unified p-value is the *exact* expectation of the Euler characteristic of the excursion set, the set of voxels where the statistical field exceeds t, for *all* thresholds t (see Worsley *et al.* 1992). The difference between the results of the latter and those presented here is that the Euler characteristic used here counts connected regions of the excursion set even if they touch the boundary of the search region, whereas the Euler characteristic used in Worsley *et al.* (1992) counted fractional values for such regions. The $d = 0, 1, 2$ terms in the unified formula are, in effect, boundary corrections that account for when the excursion set touches the boundary of the search region.

It must be remembered that the unified p-value (3.1) is still only an approximation, albeit a more accurate one than earlier approximations (Friston *et al.*, 1991; Worsley *et al.* 1992). The approximation appears to be most accurate when the search region is convex. Thus the more convoluted a surface the less (3.1) approximates the true significance. One cannot apply it, for example, to a region with a very thin invagination (such as a sulcus) which has essentially the same volume but a much larger surface area. The invagination doesn't change the likelihood of a false positive in such a region but (3.1) predicts a much greater apparent p-value. Thus there is no advantage to applying (3.1) to highly folded surfaces for the purposes of decreasing the volume and thereby decreasing the p-value, since this simultaneously increases the surface area. In such cases it is better to surround the region with a smoother envelope, at a small cost in volume, but a greater saving in surface area and p-value (3.1).

In the Appendix we show that the sensitivity of the statistical field at detecting changes in CBF can be reduced if the degrees of freedom of the variance estimator is too low. To overcome this it is clearly desirable to obtain an estimator of the variance with high degrees of freedom. Friston *et al.* (1991) proposed a variance estimator pooled across subjects and conditions; Worsley *et al.* (1992) proposed a variance estimator pooled across subjects and voxels. Both estimators are susceptible to departures from the underlying assumptions that will affect the specificity of the statistical field: that of Friston *et al.* (1991) to unequal condition variances; that of Worsley *et al.* (1992) to unequal voxel variances. It can be shown, fortunately, that neither estimator is affected by unequal subject variances, although the sensitivity of the statistical field is slightly reduced. However it is undoubtedly true that condition variances are unequal, and it is undoubtedly true that voxel variances are unequal; the real question is how severely these departures from equality affect the specificity of the statistical field. In the Appendix we show that the voxel pooled statistical field will tolerate up to 8% fluctuations in the voxel standard deviation, and the condition pooled statistical field will tolerate up to 6% fluctuations in the condition standard deviation in a typical experiment. Unfortunately it is very difficult to estimate what the true fluctuations are,

unless data is pooled over a very large number of images, so we do not know if the above limits are respected. This raises new problems; are we pooling over truly comparable images? Ultimately, some compromise must inevitably be found between an accurate specificity (by using low degrees of freedom) and a high sensitivity (by using high degrees of freedom); it is not possible to have both.

A Appendix

A.1 Regression models

The above theory can easily be extended to statistical fields that test for correlation between regressor variables, measured for each subject, and the subject responses at each voxel. The regressor variables might be, for example, age, sex (0=male, 1=female), disease (0=disease free, 1=diseased), stress measure, or even the ΔCBF measured at a particular voxel of interest (Friston *et al.* 1990). The analysis is then equivalent to repeating a multiple regression for each voxel. Suppose there are k regressors, including the constant term, and let $\mathbf{U}$ be the design matrix for the multiple regression, that is, an $n \times k$ matrix whose rows $\mathbf{u}_i'$ are the values of the k regressor variables for subject i, and prime denotes transpose. Then the ANOVA model becomes:

$$Y_{ij}(x,y,z) = r(x,y,z) + a_i(x,y,z) + \mathbf{u}_i'\delta_j(x,y,z) + \epsilon_{ij}(x,y,z) \tag{A.1}$$

where $\delta_j(x,y,z)$ is now a k-vector of CBF responses to each of the k regressor variables. For a particular contrast, let $\mathbf{V}(x,y,z)$ be the n-vector of all subject $\Delta_i(x,y,z)$ values. Then the k-vector of normalised contrast effects on the regressors is

$$\mathbf{\Delta}(x,y,z) = \mathrm{diag}[(\mathbf{U}'\mathbf{U})^{-1}]^{-1/2}(\mathbf{U}'\mathbf{U})^{-1}\mathbf{U}'\mathbf{V}(x,y,z). \tag{A.2}$$

Suitable estimators of the variance of each component of $\mathbf{\Delta}(x,y,z)$ can be found as follows. For pooling across conditions, let $\mathbf{Y}_j(x,y,z)$ be the n-vector of $Y_{ij}(x,y,z)$ values for each subject, and let $\bar{\mathbf{Y}}_\bullet(x,y,z)$ be the n-vector of $\bar{Y}_{i\bullet}(x,y,z)$ values for each subject. Then

$$s^2(x,y,z) = \sum_{i=1}^{n}\sum_{j=1}^{m}\{Y_{ij}(x,y,z) - \bar{Y}_{i\bullet}(x,y,z) - \mathbf{u}_i'(\mathbf{U}'\mathbf{U})^{-1}\mathbf{U}'[\mathbf{Y}_j(x,y,z) - \bar{\mathbf{Y}}_\bullet(x,y,z)]\}^2/\nu, \tag{A.3}$$

where $\nu = (n-k)(m-1)$, is an unbiased estimator of the variance of each component of $\mathbf{\Delta}(x,y,z)$. Dividing each component of $\mathbf{\Delta}(x,y,z)$ by this $s(x,y,z)$ will give a set of t statistical fields with ν degrees of freedom, one for each of the k regressors. For pooling across voxels, let

$$S_c^2 = \sum_{i=1}^{n}\sum_{x,y,z}[\Delta_i(x,y,z) - \mathbf{u}_i'(\mathbf{U}'\mathbf{U})^{-1}\mathbf{U}'\mathbf{V}(x,y,z)]^2/[(n-k)N]. \tag{A.4}$$

Dividing each component of $\mathbf{\Delta}(x,y,z)$ by this S_c will give a set of Gaussian statistical fields. Finally, for the combined estimator, let S^2 be the average over voxels of $s^2(x,y,z)$. Then dividing each component of $\mathbf{\Delta}(x,y,z)$ by $[S_c/S]s(x,y,z)$ will give a set of t statistical fields each with ν degrees of freedom. Note, however, that the statistical fields for different regressors may be correlated.

A.2 Robustness to incorrect standard deviations

In this section we analyse the consequences of departures from the assumed models (2.12) and (2.16) for the variances of the observations. To do this we shall examine the specificity of M when the true model is the multiplicative model (2.19).

If we assume (2.12) and pool over conditions, then the expectation of $s^2(x, y, z)$ is $v_c^2\sigma^2(x, y, z)$ where v_c^2 is the ratio of the condition variance to the average variance over all conditions. The estimator is biased unless $v_c = 1$, which will be assured if the condition variances are equal and the covariances are zero. If we use a critical value t given by the unified formula applied to $T(x, y, z)$, then the true specificity is given by the unified p-value at t/v_c. For a spherical search region of radius 6.2cm with FWHM=20mm, $\nu = 40$ degrees of freedom and $t = 4.81$ chosen for 5% specificity, a value of $v_c = 1.06$ increases the specificity to 10%. Thus a change of 6% in condition standard deviation can double the specificity.

To study the affects of pooling across voxels, we model the true variance $\sigma^2(x, y, z)$ as $[(\eta - 2)/U(x, y, z)]\sigma^2$, where $U(x, y, z)$ is an independent χ^2 field with η degrees of freedom. The pooled variance is then σ^2, and its root mean square error is $\sigma^2\sqrt{2/(\eta - 4)}$. If we use a critical value t given by the unified formula applied to $Z(x, y, z)$, then the true specificity is given by the unified formula applied to a t-statistical field with η degrees of freedom and threshold $t\sqrt{\eta/(\eta - 2)}$. For a 1000cc spherical search region with FWHM=20mm and $t = 4.16$ chosen for 5% specificity, a value of $\eta = 87$ increases the specificity to 10%. Thus a root mean square error of approximately $\sigma\sqrt{2/(\eta - 4)}/2 = 0.08\sigma$, or 8%, in the voxel standard deviation can double the specificity.

The conclusion is that departures from equal standard deviations affect both pooling methods to about the same extent; note however that pooling across voxels always increases the specificity on average, whereas pooling across conditions may increase or may decrease the specificity.

A.3 Effect of degrees of freedom on sensitivity

In this section we try to quantify the reduction in sensitivity caused by using small degrees of freedom for the variance estimator. We do this by comparing the peak heights h of the activations that can be detected with 50% sensitivity. If h is large then the maximum of the statistical field is very likely to occur at the maximum of the underlying activation. Thus the sensitivity is at least the probability that the statistical field at a single voxel exceeds the critical value for M (see Siegmund & Worsley, 1995). For a Gaussian statistical field, the sensitivity is 0.5 when h equals the Gaussian critical value. For a t statistical field the sensitivity is 0.5 when h is slightly less than the t critical value; the exact value is the median of the non-central t distribution. Thus the ratio of the peak heights that can be detected with 50% sensitivity is approximately the ratio of the critical values. For a 1000cc sphere and a 20mm FWHM, the critical values can be read off from Figures 2 and 3. At 5% specificity they are 4.16 for a Gaussian field and 4.81 for a t field with 40 degrees of freedom. The corresponding peak activations are 4.16 and 4.78, and so the ratio of peak heights is 1.15. Thus the signal has to be 15% higher before the t statistical field with 40 degrees can detect it. If the signal heights are the same then this translates into a 32% increase in the number of subjects. For 8 degrees of freedom the critical value is 12.7 and the ratio of peak heights

is 2.9, so the signal has to be nearly three times larger to be detected with a t statistical field.

A.4 Approximating the t field with a Gaussian field

Because the exact t field results in Table 2(b) were not available at the time, Friston *et al.* (1991) transformed the t field to Gaussian variables at each voxel and used the Gaussian results in Table 2(a) as an approximation. Although the resulting field is Gaussian at each voxel, it is not strictly a *Gaussian field* (a Gaussian field must also be multivariate Gaussian at every set of voxels), although it does converge to a Gaussian field for large degrees of freedom. Some idea of how large ν must be for this to be accurate can be obtained by comparing the nominal false positive rate given by a Gaussian transformation followed by using the Gaussian results in Table 2(a) with the true false positive rate given by the t results in Table 2(b). For a 0.05 nominal false positive rate, $\nu = 40$ degrees of freedom, a 1000cc spherical search region and a 20mm FWHM, the true false positive rate is increased to 0.069. For the same test with $\nu = 120$ degrees of freedom, the true false positive rate is 0.055; this is approximately the same as that obtained by using the Gaussian tables instead of the t tables in an ordinary t test with 30 degrees of freedom. Since 30 degrees of freedom is usually considered large enough to approximate the t by a Gaussian distribution, then $\nu = 120$ degrees of freedom should be large enough to approximate the Gaussianised t field by a Gaussian field.

A.5 χ^2 and F statistical fields

A χ^2 field with ν degrees of freedom is defined as the sum of squares of ν independent zero mean, unit variance Gaussian fields. An example is the statistical field $\nu s^2(x, y, z)/S^2$, if the assumptions in Section 2.3 hold. If these assumptions do not hold, then peaks in such a statistical field would indicate regions of high or low voxel variance. Another application is to combine Gaussian statistical fields either from k different conditions or regressors, looking for activation due to some or all conditions or regressors. The sum of squares of these Gaussian statistical fields is then a χ^2 field with k degrees of freedom. If the denominator error variance is not pooled across voxels, but is based on pooling across conditions, then the ratio of mean sum of squares is an F field with k and ν degrees of freedom. In either case the same unified p-value can be used but with the EC densities given in Table 2(c) and Table 2(d). For p-values of minima of either the χ^2 or F statistical fields, $\rho_0(t)$, $\rho_2(t)$ and $\rho_4(t)$ should be replaced by $1 - \rho_0(t)$, $-\rho_2(t)$ and $-\rho_4(t)$, respectively.

Acknowledgement

K.J. Worsley was supported by the Natural Sciences and Engineering Research Council of Canada, and the Fonds pour la Formation des Chercheurs et l'Aide à la Recherche de Québec.

References

Adler RJ, (1981): *The Geometry of Random Fields.* New York: Wiley.

Evans AC, Marrett S, Neelin P, Collins L, Worsley KJ, Dai W, Milot S, Meyer E, Bub D, (1992): Anatomical mapping of functional activation in stereotactic coordinate space. *Neuro Image* **1**:43-53.

Evans AC, Marrett S, Torrescorzo J, Ku S, Collins L, (1991a): MRI-PET correlative analysis using a volume of interest (VOI) atlas. *Journal of Cerebral Blood Flow and Metabolism* **11(2)**:A69-A78.

Fox PT, Mintun MA, Reiman EM, Raichle ME, (1988): Enhanced detection of focal brain responses using intersubject averaging and distribution analysis of subtracted PET images. *Journal of Cerebral Blood Flow and Metabolism* **8**:642-653.

Fox PT, Perlmutter JS, Raichle ME, (1985): A stereotactic method of anatomical localization for positron emission tomography. *Journal of Computer Assisted Tomography* **9(1)**:141-153.

Friston KJ, Frith CD, Liddle PF, Frackowiak RSJ, (1991): Comparing functional (PET) images: the assessment of significant change *Journal of Cerebral Blood Flow and Metabolism* **11**:690-699.

Friston KJ, Frith CD, Liddle PF, Lammertsma AA, Dolan RD, Frackowiak RSJ, (1990): The relationship between local and global changes in PET scans. *Journal of Cerebral Blood Flow and Metabolism* **10**:458-466.

Friston KJ, Jezzard P, Turner R, (1994a): Analysis of functional MRI time series. *Human Brain Mapping* **1**:153-171.

Friston KJ, Holmes AP, Worsley KJ, Poline J-B, Frith CD, Frackowiak RSJ, (1994b): Statistical parametric maps in functional imaging: A general approach. (in preparation).

Kwong KK, Belliveau JW, Chesler DA, Goldberg IE, Weisskoff RM, Poncelet BP, Kennedy DN, Hoppel BE, Cohen MS, Turner R, Cheng H-M, Brady TJ, Rosen BR, (1992): Dynamic magnetic resonance imaging of human brain activity during primary sensory stimulation. *Proceedings of the Nationol Academy of Science* **89:**5675-5679.

Ogawa S, Tank DW, Menon R, Ellerman JM, Kim S-G, Merkle H, Ugurbil K, (1992): Intrinsic signal changes accompanying sensory stimulation: functional brain mapping with magnetic resonance imaging. *Proceedings of the Nationol Academy of Science* **89:**5951-5955.

Ouyang X, Pike GB, Evans AC, (1994): fMRI of human visual cortex using temporal correlation and spatial coherence analysis. *13th Annual Symposium of the Society of Magnetic Resonance in Medicine.*

Santaló LA, (1976): *Integral Geometry and Geometric Probability. In: Rota, G-C (ed): Encyclopedia of Mathematics and its Applications, Volume 1.* Reading, Massachusetts: Addison-Wesley.

Siegmund DO, Worsley KJ, (1994): Testing for a signal with unknown location and scale in a stationary Gaussian random field. *Annals of Statistics* to appear.

Talbot JD, Marrett S, Evans AC, Meyer E, Bushnell MC, Duncan GH, (1991): Multiple representations of pain in human cerebral cortex. *Science* **251**:1355-1358.

Worsley KJ, Evans AC, Marrett S, Neelin P, (1992): A three dimensional statistical analysis for CBF activation studies in human brain. *Journal of Cerebral Blood Flow and Metabolism* **12**:900-918.

Worsley KJ, Evans AC, Marrett S, Neelin P, (1993): Detecting and estimating the regions of activation in CBF activation studies in human brain. *In: Uemura K, Lassen NA, Jones T, Kanno, I (eds): Quantification of Brain Function: Tracer kinetics and image analysis in brain PET.* Tokyo: Excerpta Medica, pp. 535-548.

Worsley KJ, (1994): Local maxima and the expected Euler characteristic of excursion sets of χ^2 F and t fields. *Advances in Applied Probability* **26**:13-42.

Worsley KJ, (1995a): Estimating the number of peaks in a random field using the Hadwiger characteristic of excursion sets with applications to medical images. *Annals of Statistics*, in press.

Worsley KJ, (1995b): Boundary corrections for the expected Euler characteristic of excursion sets of random fields, with an application to astrophysics. *Advances in Applied Probability*, in press.

TABLE 1. Resel counts for some simple shapes

Search region V in resel space	Resel counts $R_0(V)$	$R_1(V)$	$R_2(V)$	$R_3(V)$
Sphere, radius r	1	$4r$	$2\pi r^2$	$(4/3)\pi r^3$
Hemisphere, radius r	1	$(2+\pi/2)r$	$(3/2)\pi r^2$	$(2/3)\pi r^3$
Disk, radius r	1	πr	πr^2	0
Hemisphere surface, radius r	1	πr	$2\pi r^2$	0
Box, $a \times b \times c$	1	$a+b+c$	$ab+bc+ac$	abc
Rectangle, $a \times b$	1	$a+b$	ab	0
Line, length a	1	a	0	0

TABLE 2. EC densities $\rho_d(t)$ in d dimensions

(a) Gaussian field

$$\begin{aligned}
\rho_0(t) &= \int_t^\infty \frac{1}{(2\pi)^{\frac{1}{2}}} e^{-u^2/2} du \\
\rho_1(t) &= \frac{(4\log_e 2)^{\frac{1}{2}}}{2\pi} e^{-t^2/2} \\
\rho_2(t) &= \frac{(4\log_e 2)}{(2\pi)^{\frac{3}{2}}} e^{-t^2/2} t \\
\rho_3(t) &= \frac{(4\log_e 2)^{\frac{3}{2}}}{(2\pi)^2} e^{-t^2/2}(t^2-1) \\
\rho_4(t) &= \frac{(4\log_e 2)^2}{(2\pi)^{\frac{5}{2}}} e^{-t^2/2}(t^3-3t)
\end{aligned}$$

(b) t field with ν degrees of freedom, $\nu \geq d$

$$\begin{aligned}
\rho_0(t) &= \int_t^\infty \frac{\Gamma\left(\frac{\nu+1}{2}\right)}{(\nu\pi)^{\frac{1}{2}}\Gamma\left(\frac{\nu}{2}\right)} \left(1+\frac{u^2}{\nu}\right)^{-\frac{1}{2}(\nu+1)} du \\
\rho_1(t) &= \frac{(4\log_e 2)^{\frac{1}{2}}}{2\pi} \left(1+\frac{t^2}{\nu}\right)^{-\frac{1}{2}(\nu-1)} \\
\rho_2(t) &= \frac{(4\log_e 2)}{(2\pi)^{\frac{3}{2}}} \frac{\Gamma\left(\frac{\nu+1}{2}\right)}{\left(\frac{\nu}{2}\right)^{\frac{1}{2}}\Gamma\left(\frac{\nu}{2}\right)} \left(1+\frac{t^2}{\nu}\right)^{-\frac{1}{2}(\nu-1)} t \\
\rho_3(t) &= \frac{(4\log_e 2)^{\frac{3}{2}}}{(2\pi)^2} \left(1+\frac{t^2}{\nu}\right)^{-\frac{1}{2}(\nu-1)} \left(\frac{\nu-1}{\nu}t^2-1\right) \\
\rho_4(t) &= \frac{(4\log_e 2)^2}{(2\pi)^{\frac{5}{2}}} \frac{\Gamma\left(\frac{\nu+1}{2}\right)}{\left(\frac{\nu}{2}\right)^{\frac{1}{2}}\Gamma\left(\frac{\nu}{2}\right)} \left(1+\frac{t^2}{\nu}\right)^{-\frac{1}{2}(\nu-1)} \left(\frac{\nu-2}{\nu}t^3-3t\right)
\end{aligned}$$

(c) χ^2 field with ν degrees of freedom

$$\begin{aligned}
\rho_0(t) &= \int_t^\infty \frac{u^{\frac{1}{2}(\nu-2)}e^{-\frac{1}{2}u}}{2^{\frac{\nu}{2}}\Gamma\left(\frac{\nu}{2}\right)}du \\
\rho_1(t) &= \frac{(4\log_e 2)^{\frac{1}{2}}}{(2\pi)^{\frac{1}{2}}}\frac{t^{\frac{1}{2}(\nu-1)}e^{-\frac{1}{2}t}}{2^{\frac{1}{2}(\nu-2)}\Gamma\left(\frac{\nu}{2}\right)} \\
\rho_2(t) &= \frac{(4\log_e 2)}{(2\pi)}\frac{t^{\frac{1}{2}(\nu-2)}e^{-\frac{1}{2}t}}{2^{\frac{1}{2}(\nu-2)}\Gamma\left(\frac{\nu}{2}\right)}[t-(\nu-1)] \\
\rho_3(t) &= \frac{(4\log_e 2)^{\frac{3}{2}}}{(2\pi)^{\frac{3}{2}}}\frac{t^{\frac{1}{2}(\nu-3)}e^{-\frac{1}{2}t}}{2^{\frac{1}{2}(\nu-2)}\Gamma\left(\frac{\nu}{2}\right)}[t^2-(2\nu-1)t+(\nu-1)(\nu-2)] \\
\rho_4(t) &= \frac{(4\log_e 2)^2}{(2\pi)^2}\frac{t^{\frac{1}{2}(\nu-4)}e^{-\frac{1}{2}t}}{2^{\frac{1}{2}(\nu-2)}\Gamma\left(\frac{\nu}{2}\right)}[t^3-3\nu t^2+3(\nu-1)^2t-(\nu-1)(\nu-2)(\nu-3)]
\end{aligned}$$

(d) F field with k and ν degrees of freedom, $k+\nu > d$

$$\begin{aligned}
\rho_0(t) &= \int_t^\infty \frac{\Gamma\left(\frac{\nu+k-2}{2}\right)}{\Gamma\left(\frac{\nu}{2}\right)\Gamma\left(\frac{k}{2}\right)}\frac{k}{\nu}\left(\frac{ku}{\nu}\right)^{\frac{1}{2}(k-2)}\left(1+\frac{ku}{\nu}\right)^{-\frac{1}{2}(\nu+k)}du \\
\rho_1(t) &= \frac{(4\log_e 2)^{\frac{1}{2}}}{(2\pi)^{\frac{1}{2}}}\frac{\Gamma\left(\frac{\nu+k-1}{2}\right)2^{\frac{1}{2}}}{\Gamma\left(\frac{\nu}{2}\right)\Gamma\left(\frac{k}{2}\right)}\left(\frac{kt}{\nu}\right)^{\frac{1}{2}(k-1)}\left(1+\frac{kt}{\nu}\right)^{-\frac{1}{2}(\nu+k-2)} \\
\rho_2(t) &= \frac{(4\log_e 2)}{2\pi}\frac{\Gamma\left(\frac{\nu+k-2}{2}\right)}{\Gamma\left(\frac{\nu}{2}\right)\Gamma\left(\frac{k}{2}\right)}\left(\frac{kt}{\nu}\right)^{\frac{1}{2}(k-2)}\left(1+\frac{kt}{\nu}\right)^{-\frac{1}{2}(\nu+k-2)} \\
&\times \left[(\nu-1)\frac{kt}{\nu}-(k-1)\right] \\
\rho_3(t) &= \frac{(4\log_e 2)^{\frac{3}{2}}}{(2\pi)^{\frac{3}{2}}}\frac{\Gamma\left(\frac{\nu+k-3}{2}\right)2^{-\frac{1}{2}}}{\Gamma\left(\frac{\nu}{2}\right)\Gamma\left(\frac{k}{2}\right)}\left(\frac{kt}{\nu}\right)^{\frac{1}{2}(k-3)}\left(1+\frac{kt}{\nu}\right)^{-\frac{1}{2}(\nu+k-2)} \\
&\times \left[(\nu-1)(\nu-2)\left(\frac{kt}{\nu}\right)^2-(2\nu k-\nu-k-1)\left(\frac{kt}{\nu}\right)+(k-1)(k-2)\right] \\
\rho_4(t) &= \frac{(4\log_e 2)^2}{(2\pi)^2}\frac{\Gamma\left(\frac{\nu+k-4}{2}\right)2^{-1}}{\Gamma\left(\frac{\nu}{2}\right)\Gamma\left(\frac{k}{2}\right)}\left(\frac{kt}{\nu}\right)^{\frac{1}{2}(k-4)}\left(1+\frac{kt}{\nu}\right)^{-\frac{1}{2}(\nu+k-2)} \\
&\times \left[(\nu-1)(\nu-2)(\nu-3)\left(\frac{kt}{\nu}\right)^3-3(\nu-1)(\nu k-k-2)\left(\frac{kt}{\nu}\right)^2\right. \\
&+ \left. 3(k-1)(k\nu-\nu-2)\left(\frac{kt}{\nu}\right)-(k-1)(k-2)(k-3)\right]
\end{aligned}$$

TABLE 3. Representative examples of resel counts and critical values.

Search region V	Vol. (cc)	Resel counts $R_0(V)$	$R_1(V)$	$R_2(V)$	$R_3(V)$	t for P($M \geq t$) = 0.10	0.05	0.01
Single voxel	0	1	0	0	0	1.28	1.64	2.33
Head Of Caudate	7	0	6.18	4.63	0.65	2.75	3.02	3.55
Putamen	12	1	7.32	6.80	1.18	2.89	3.15	3.66
Globus Pallidus	3	0	4.03	2.29	0.24	2.49	2.78	3.35
Thalamus	11	1	4.94	5.14	1.13	2.79	3.05	3.59
Anterior Cingulate Gyrus	9	1	8.20	5.79	0.86	2.86	3.11	3.63
Posterior Cingulate Gyrus	6	1	5.32	3.85	0.58	2.70	2.97	3.51
Cingulate Gyri	15	0	12.89	9.63	1.44	3.03	3.27	3.77
Superior Frontal Gyrus	80	1	15.64	25.69	8.97	3.38	3.60	4.07
Middle Frontal Gyrus	57	1	14.89	21.14	6.23	3.31	3.53	4.00
Inferior Frontal Gyrus	37	1	11.22	14.25	4.06	3.17	3.41	3.89
Precentral Gyrus	32	1	12.30	14.23	3.40	3.16	3.40	3.88
Frontal Gyri	207	1	19.30	53.39	23.63	3.63	3.84	4.28
Postcentral Gyrus	27	1	10.59	12.56	2.89	3.11	3.35	3.84
Superior Parietal Lobule	22	1	7.95	9.89	2.34	3.03	3.27	3.77
Supramarginal Gyrus	19	1	7.27	7.72	2.00	2.95	3.21	3.72
Angular Gyrus	20	1	6.56	8.20	2.14	2.96	3.22	3.73
Paracentral Lobule	14	1	6.35	7.03	1.49	2.90	3.16	3.67
Precuneus	26	1	8.75	10.26	2.80	3.06	3.30	3.80
Parietal lobe	128	1	15.20	37.04	14.49	3.50	3.72	4.17
Superior Temporal Gyrus	40	0	13.75	16.70	4.24	3.22	3.45	3.93
Middle Temporal Gyrus	39	0	14.33	16.43	4.16	3.22	3.45	3.93
Inferior Temporal Gyrus	25	1	8.61	10.32	2.63	3.05	3.30	3.79
Occipitotemporal Gyrus	13	1	8.99	7.58	1.32	2.94	3.19	3.70
Temporal Gyri	117	0	16.99	36.70	13.03	3.49	3.71	4.16
Lateral Occipitotemporal Gyrus	23	-1	10.12	11.16	2.41	3.06	3.31	3.80
Medial Occipitotemporal Gyrus	5	1	3.96	2.93	0.44	2.58	2.86	3.42
Occipital Gyrus	12	1	6.90	6.54	1.25	2.88	3.14	3.65
Cuneus	19	1	6.85	8.04	2.05	2.96	3.21	3.72
Lingual Gyrus	6	1	4.86	3.69	0.59	2.68	2.95	3.49
Occipital Lobe	65	-1	10.68	23.11	7.17	3.32	3.55	4.02
4mm shell	254	2	0.54	207.27	15.88	3.85	4.04	4.45
Whole brain	1294	1	20.43	107.09	153.42	4.05	4.23	4.63

Figure 1. Example of resel coefficients

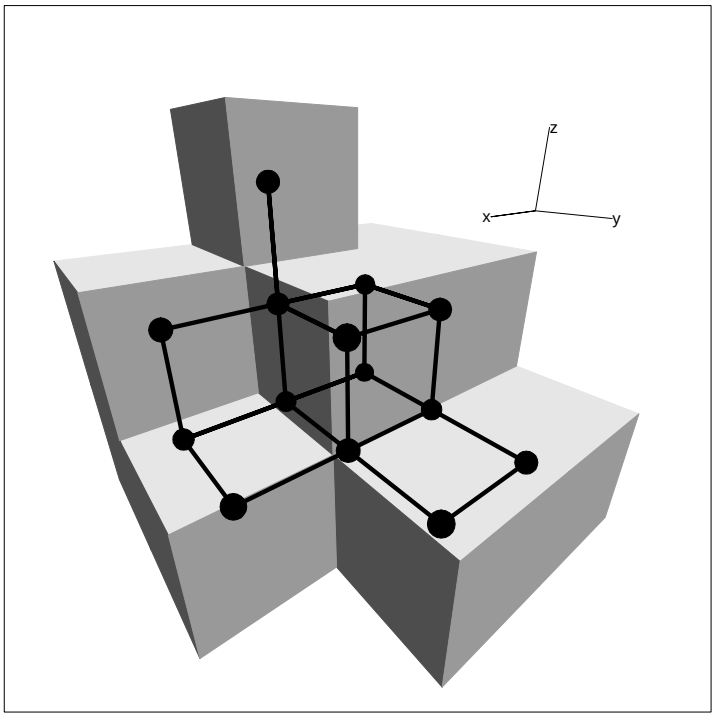

Figure 1: Example of resel counts. The voxels of a search region V are indicated by shaded cubes, and their centres are indicated by black spheres. Adjacent voxels are joined by heavy black lines. Then P=14, E_x=8, E_y=7, E_z=6, F_{xy}=4, F_{xz}=3, $F_{yz}=2$ and C=1. If the voxel separations are equal, that is $\delta_x = \delta_y = \delta_z = \delta$, then this gives $R_0(V) = 1$, $R_1(V) = 6\delta$, $R_2(V) = 6\delta^2$ and $R_3(V) = \delta^3$.

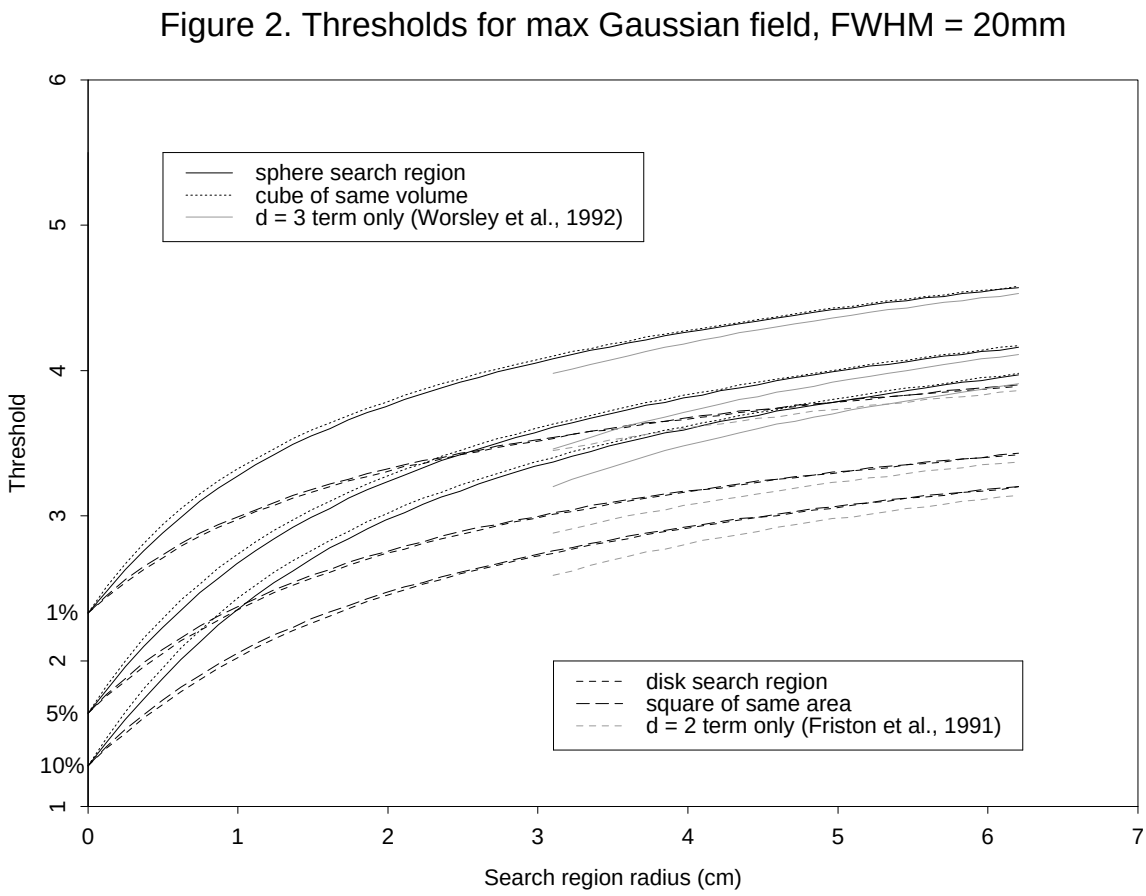

Figure 2: Theoretical critical thresholds for the maximum of a Gaussian statistical field with FWHM=20mm based on the unified p-value (3.1), plotted against the radius of a spherical search region, together with critical thresholds for a cube of the same volume, a disk, and a square of the same area. The false positive rates are 1%, 5% and 10%. Also shown are the critical thresholds based on the $d = 3$ term (Worsley *et al.* 1992) and the $d = 2$ term (Friston *et al.* 1991) which are accurate only for large region sizes.

Figure 3. Thresholds for max t field, 40 d.f., FWHM = 20mm

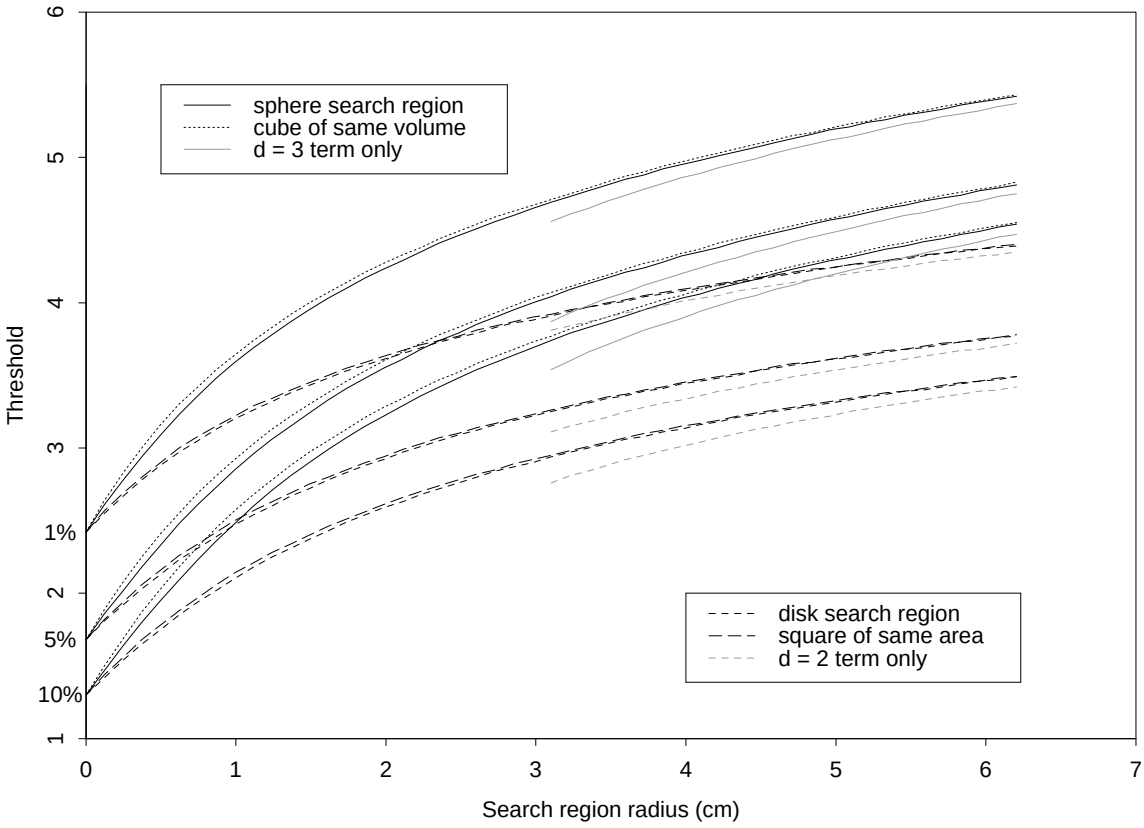

Figure 3: As for Figure 2, but for a t statistical field with 40 degrees of freedom.

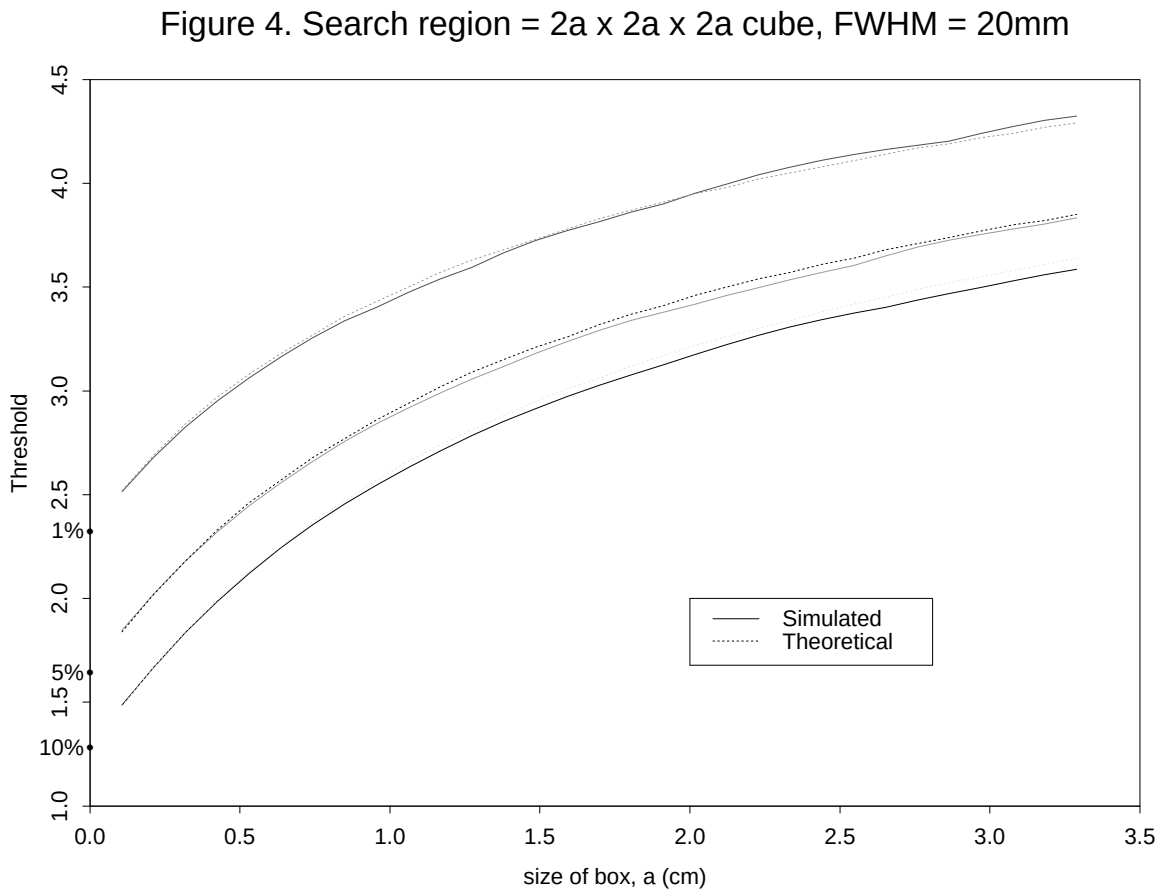

Figure 4: Simulated and theoretical critical thresholds for the maximum of a Gaussian statistical field with FWHM=20mm inside a $2a \times 2a \times 2a$ cube. The false positive rates are 1%, 5% and 10%.

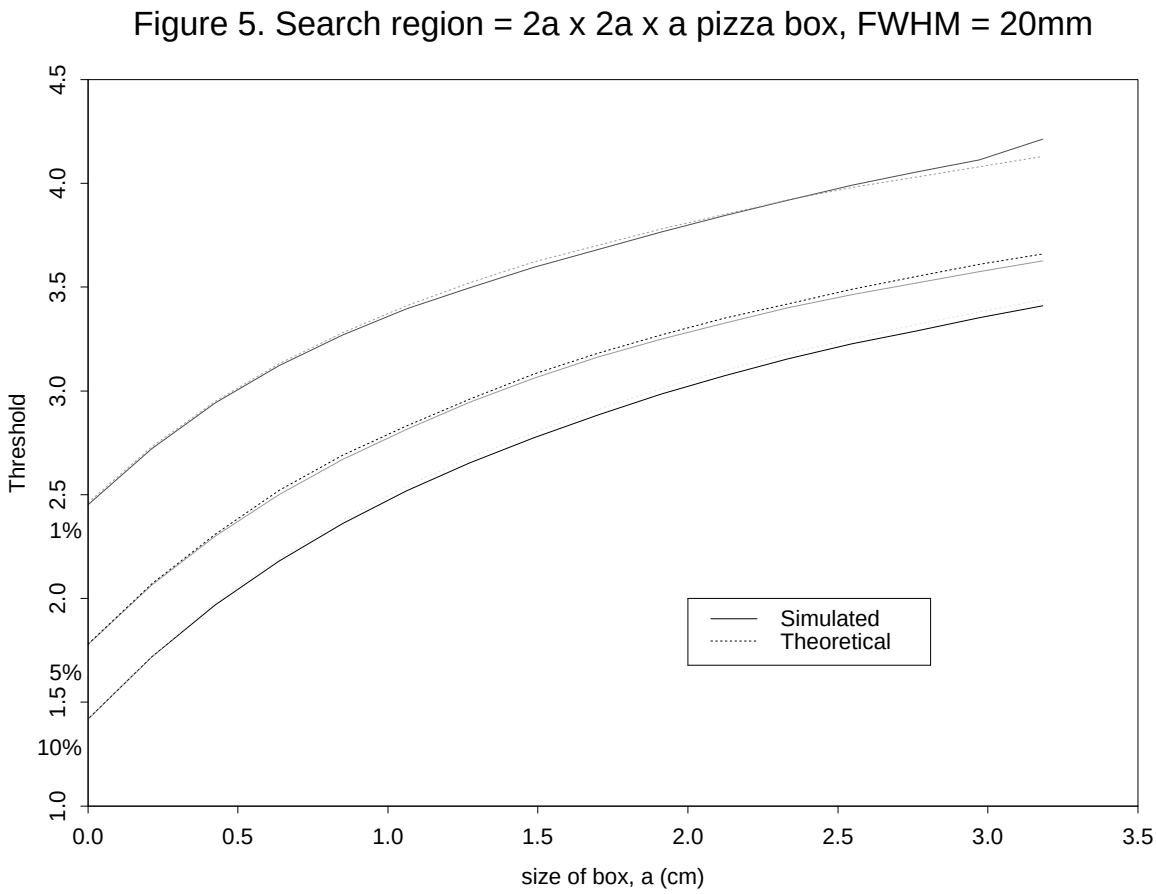

Figure 5: Simulated and theoretical critical thresholds for the maximum of a Gaussian statistical field with FWHM=20mm inside a $2a \times 2a \times a$ 'pizza box'. The false positive rates are 1%, 5% and 10%.

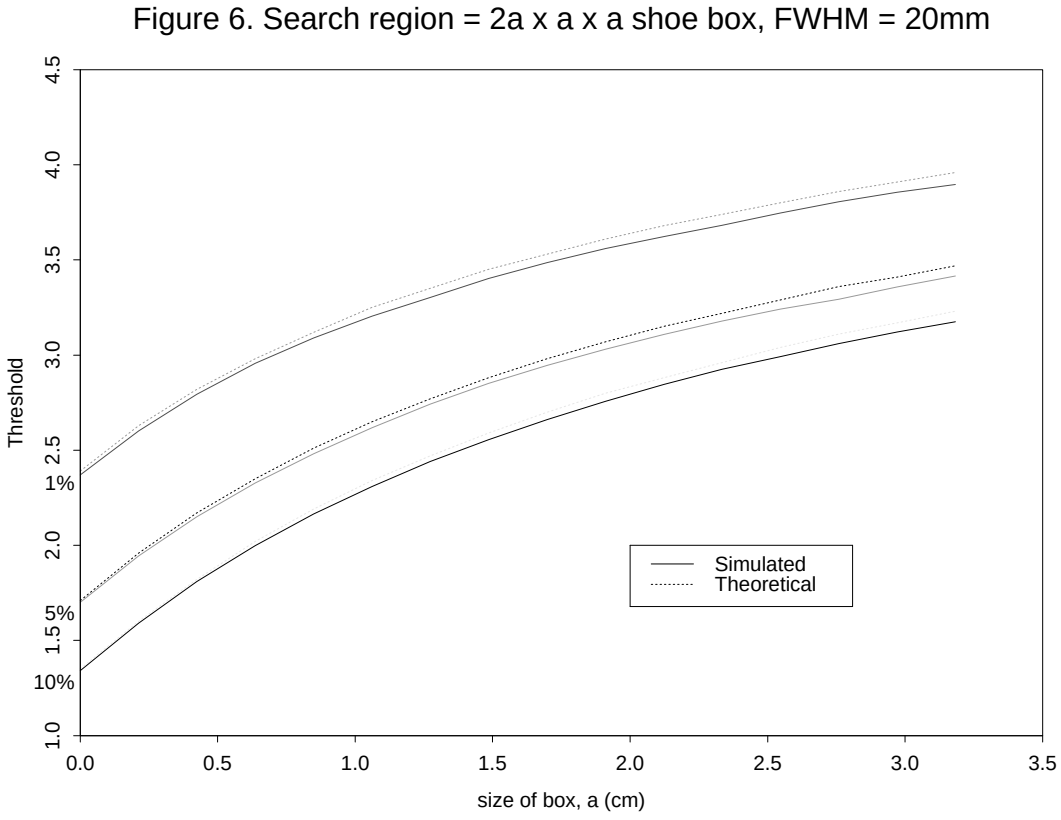

Figure 6: Simulated and theoretical critical thresholds for the maximum of a Gaussian statistical field with FWHM=20mm inside a $2a \times a \times a$ 'shoe box'. The false positive rates are 1%, 5% and 10%.